Available online at www.ijrp.org

IJRP.ORG
International Journal of Research Publications
ISSN: 2708-3578 (Online)

International Journal of Research Publications

Volume-14, Issue-1,October 2018

ISSN number 2708-3578 (Online)

Accepted and Published Manuscript

Analytical Device Model of Graphene Nanoribbon Field Effect Transistor

Md. Rakibul Alam, Md. Imran Hossain, Jannatul Ferdous, Dr. Md Iqbal Bahar Chowdhury

PII : Md. Rakibul Alam.100141102018387
DOI: 100141102018387
Web: https://ijrp.org/paper-detail/388

To appear in: International Journal of Research Publication (IJRP.ORG)

Received date: 06 Oct 2018
Accepted date: 15 Oct 2018
Published date: 27 May 2022

Please cite this article as: Md. Rakibul Alam, Md. Imran Hossain, Jannatul Ferdous, Dr. Md Iqbal Bahar Chowdhury , Analytical Device Model of Graphene Nanoribbon Field Effect Transistor , International Journal of Research Publication (Volume: 14, Issue: 1), https://ijrp.org/paper-detail/388

IJRP.ORG
International Journal of Research Publications
ISSN: 2708-3578 (Online)

Analytical Device Model of Graphene Nanoribbon Field Effect Transistor

Md. Rakibul Alam[a]*, Md. Imran Hossain[a], Jannatul Ferdous[a], Dr. Md Iqbal Bahar Chowdhury[a]

[a]*Department of Electrical and Electronic Engineering, United International University, Dhaka, Bangladesh*
**Corresponding Author: Lecturer, Sonargaon University, 147/I Green road, Dhaka, Bangladesh*

Abstract

The mobility of electron denotes how quickly electron can move through any metal or semiconductor, when pulled by an electric field. In our work, we present an analytical device model specially for a Graphene Nanoribbon Field Effect Transistor (GNRFET). A highly conducting substrate whose mobility is very high plays a vital role of the back gate, but the top gate tends to control the drain current. In our model, we calculated the potential distributions in the GNRFET as a function of back gate voltage, top gate voltage and drain voltage.
Keywords: Graphene Nanoribbon, GNRFET, Back gate voltage, Top gate voltage, Drain voltage, Drain current.

1. Introduction

Graphene Nanoribbons (GNRs) consists of one-dimensional structures with hexagonal two-dimensional carbon lattices, which are stripes of Graphene. GNR is obtained from Graphenesheet. GNRs demonstrate low scattering effects inspite of being very small the width of the ribbon.

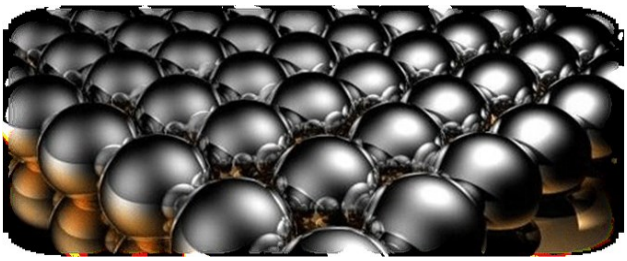

Fig. 1. Graphene Nanoribbon

The electronic states of GNRs highly depend on the edge structures (armchair or zigzag). Firstly, in zigzag edges each successive edge segment is at the opposite angle to the previous. Secondly, in armchair edges, each pair of segments is a 120° or -120° rotation of the prior pair. Zigzag edges provide the edge localized state with non-bonding molecular orbitals near the Fermi energy and they are expected to have large variations in optical and electronic properties from quantization [1]. Calculations based on tight binding theory predict that zigzag GNRs are always metallic whereas armchairs can be either metallic or semiconducting, depending on their width. The Density Functional Theory (DFT) calculations show, armchair nanoribbons are semiconducting with an energy gap scaling with the inverse of the GNR width [2]. Experiments verified that energy gaps increase

with decreasing GNR width [3]. Graphene nanoribbons with controlled edge orientation have been fabricated by Scanning Tunneling Microscope (STM) lithography [4] and energy gaps up to 0.5 eV in a 2.5 nm wide armchair ribbon were reported. Zigzag nanoribbons are semiconducting. Their gap shows to an unusual antiferromagnetic coupling between the magnetic moments at opposite edge carbon atoms and this gap size is inversely proportional to the ribbon width [5,6]. The mostly local character of the exchange interaction originates the spin polarization. So, in zigzag GNR, the quantum confinement, inter-edge superexchange and intra-edge direct exchange interactions are important for its magnetism and band gap. The edge magnetic moment and band gap of zigzag GNR are reversely proportional to the electron/hole concentration. They can be controlled by alkaline adatoms [7]. The 2D structure, high electrical and thermal conductivity and the low noise also make GNRs a possible alternative to copper for Integrated Circuit (IC) interconnects. Research is exploring to make the quantum dots by changing the width of GNRs at select points along the ribbon, creating quantum confinement [8].

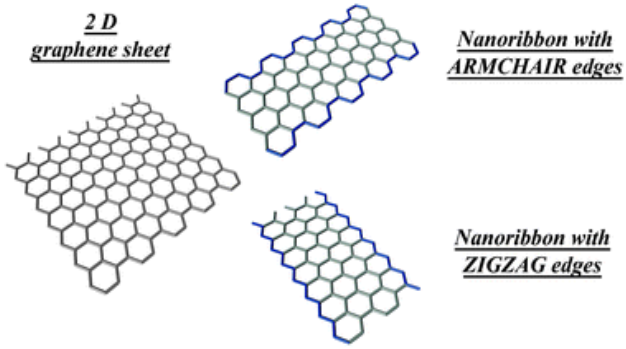

Fig. 2. 2D Graphene Sheet, Nanoribbon with Armchair and Zigzag edges

Graphene nanoribbons possess semiconductive properties. It may be a technological alternative to silicon semiconductors [9] which is capable of sustaining microprocessor clock speeds in the vicinity of 1 THz [10] Field-Effect Transistors (FETs) less than 10 nm wide have been made with GNR – "GNRFETs" – with an I_{on}/I_{off} ratio $>10^6$ at room temperature [11,12].

A GNRFET is an FET device with GNR as the channel material and the GNR sandwiched between the source and drain electrodes controlled by the gate through the gate voltage applied is illustrated in Figure 3[13]. One of the advantages of utilizing GNR as the channel material in GNRFET is its most powerful ability to control the electrostatics. GNRFET performance is evaluated through current–voltage (I–V) characteristics. Liang et al. [14], for example, calculated the I–V characteristics for ballistic GNRFET by employing the "top-of-barrier" approach. The I–V characteristics of GNRFET show better performance than the Silicon Metal–Oxide–Semiconductor Field-Effect Transistor (Si MOSFET). This is due to the higher average velocity in the GNR. Pei et al. [15] evaluated GNRFET through the analytical modeling of the current at ballistic limit. The

computation of the transmission coefficient is also included in the current model, taking into account the edge and Optical Phonon (OP) scatterings. The fabrication of GNRFET conducted by Wang et al. [11] found that gate material of palladium (Pd) yields a higher on-current (I_{on}) than titanium (Ti) and gold (Au). The GNR width effects on the I–V characteristics were studied by Choudhury et al. [16], assuming a Schottky-barrier FET. The results suggested that the current is larger for GNR with higher width and vice versa. Yan et al. [18] worked on the I–V characteristics of GNRFET by implementing first-principles transport calculations. The work carried out showed that GNRFET can achieve high performance levels similar to other FETs made of single-walled nanotubes (SWNTs).

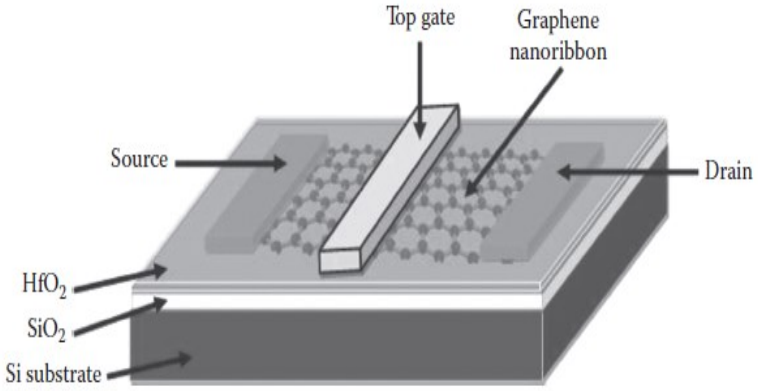

Fig. 3. Structure of a GNRFET with GNR as the channel material

Nomenclature	
Lg	Length of the top gate [nm]
Wb	Thickness of layers between graphene and the back gate [nm]
Wg	Thickness of layers between graphene and the top gate [nm]
æ	Dielectric constant of materials between the channel and gates [F/m]
Vb	The back gate voltage [V]
Vd	The potential of the drain contact [V]
Vg	The top gate voltage [V]
Ø	The electrostatic potential [V]
e	Elementary charge [Coulombs]
Ψ	The electric potential [V]
v	The characteristic velocity of the electron [cm/s]
Δ	Energy Bandgap [eV]

KB	Boltzman constant [m2kgs-2K-1]
T	Temperature [Kelvin]
J	Current density [mA/cm]
Ion	Current in on condition [A]
Ioff	Current in off condition [A]

2. Analytical device modeling for GNRFET

Graphene nanoribbons exhibit the energy spectrum with a gap between the valence and conduction bands depending on the nanoribbon width d,

$$\varepsilon_{p,n}^{-1} = \pm v\sqrt{p^2 + (\pi\hbar/d)^2\, n^2} \tag{1}$$

To find the potential distribution along the channel, we use the following equation

$$\frac{W_b+W_g}{3}\frac{\partial^2\emptyset}{\partial x^2} - \frac{\emptyset-V_b}{W_b} - \frac{\emptyset-V_g}{W_g} = \frac{4\pi e}{æ}(\sum\nolimits_- - \sum\nolimits_+) \tag{2}$$

with the boundary conditions $\emptyset|_x = -L_g/2 = 0, \emptyset|_x = -L_g/2 = V_d$

2.1 Potential Distribution

Considering that the electron and hole gases are non-degenerate and hence the electron and hole distribution functions in the sub bands with $n = 1$ near the source and drain is given by:

A. Electron and hole densities:

The application of negative top gate voltage leads to the formation of a potential barrier in the channel. This barrier calculated by the gate voltage controls the source-drain current which is responsible of the device operation as a transistor.

Since $V_b > 0$, the electron density markedly exceeds the hole density, we can neglect $\sum_h$ in the right-hand side of Eq. (2). Considering the relationships between the electron density and the electric potential, from Eq. (2) the following equations governing the potential distribution in the active region:

$$\frac{\partial^2\emptyset}{\partial x^2} - \frac{3}{W_bW_g}\emptyset = -\frac{3(V_b/W_b+V_g/W_g)}{(W_b+W_g)} + \frac{3V_b}{(W_b+W_g)W_b}exp(\frac{e\emptyset}{K_BT}) \tag{3}$$

$$\frac{\partial^2\emptyset}{\partial x^2} - \frac{3}{W_bW_g}(\emptyset - V_d) = -\frac{3(V_b/W_b+V_g/W_g)}{(W_b+W_g)} + \frac{3V_b}{(W_b+W_g)W_b}exp(\frac{e\emptyset-V_d}{K_BT}) \tag{4}$$

B. Potential distributions at low top-gate voltages

When the top gate is negative ($V_g < 0$) and its absolute value $|V_g|$ is sufficiently small, the modulus of the potential $|\emptyset|$can be not that large. In this case, we can linearize Eqs. (3) and (4) and present these equations in the following form:

$$\frac{\partial^2 \emptyset}{\partial x^2} - \frac{3}{W_b W_g}\left[1 + \frac{W_g}{W_b+W_g}\frac{eV_b}{K_B T}\right]\emptyset = \frac{3V_g}{(W_b+W_g)W_g} \tag{5}$$

$$\frac{\partial^2 \emptyset}{\partial x^2} - \frac{3}{W_b W_g}\left[1 + \frac{W_g}{W_b+W_g}\frac{e(V_b-V_d)}{K_B T}\right]\emptyset = \frac{3(V_g/W_g - V_d/W_b}{W_b+W_g} \tag{6}$$

At $V_d = 0$, Eqs. (5) and (6) yield

$$\emptyset \cong \frac{V_g W_b}{W_b+W_g}\frac{[1-\frac{\cosh(x/\lambda)}{\cosh(L_g/2\lambda)}]}{[1+\frac{W_g eV_b}{(W_b+W_g)K_B T}]} \tag{7}$$

The function exhibits a minimum $\emptyset = \emptyset_{m0}$at $x = 0$,

$$\emptyset_{m0} = \frac{V_g W_b}{W_b+W_g}\frac{[1-\frac{1}{\cosh(L_g/2\lambda)}]}{\sqrt{1+\frac{W_g eV_b}{(W_b+W_g)K_B T}}} \cong \frac{V_g W_b K_B T}{V_b W_g e} \tag{8}$$

Here, we have taken into account that normally $V_b \gg K_B T/e$

$$\emptyset_m \cong \emptyset_{m0} \cong \frac{V_g W_b K_B T}{V_b W_g e} \tag{9}$$

C. Potential distributions at high top-gate voltages

In a significant part of the active region the electron charge which is in such a situation exponentially small, can be disregarded and the last terms in Eqs. (5) and (6) can be omitted. Taking this into account, at high top gate voltages, Eqs (5) and (6) in the central region can be presented in the following form:

$$\frac{\partial^2 \emptyset}{\partial x^2} - \frac{3}{W_b W_g}\emptyset = -\frac{3(V_b/W_b + V_g/W_g)}{(W_b+W_g)} \tag{10}$$

Solving Eq. (9), we can write

$$\emptyset = \left(V_g + V_b\frac{W_b}{W_g}\right)\frac{W_b}{W_b+W_g}\left[1 - \frac{\cosh(x/\Lambda)}{\cosh(L_g/2\Lambda)}\right] + V_d\frac{\sinh(x+L_g/2)/\Lambda}{\sinh(L_g/\Lambda)} \tag{11}$$

where $\Lambda = \sqrt{W_b W_g/3}$

At $V_d = 0$, $\emptyset$ exhibits a minimum at $x = 0$,

$$\emptyset_{m0} = \left(V_g + V_b\frac{W_b}{W_g}\right)\frac{W_b}{W_b+W_g}\left[1 - \frac{1}{\cosh(L_g/2\Lambda)}\right] \tag{12}$$

At reasonable values of the drain voltage V_d,

$$\emptyset_m = \left(V_g + V_b \frac{W_b}{W_g}\right) \frac{W_b}{W_b+W_g} \left[1 - \frac{1}{\cosh\,(L_g/2\Lambda)}\right] + \frac{V_d}{2\cosh\,(L_g/2\Lambda)} \tag{13}$$

3.0 Calculation and analysis of Current-Voltage characteristics

Considering that the drain current is determined by the electrons overcoming the potential barrier under the top gate, we use the following formula for the current density:

$$J = v\left(\frac{æ}{2\pi^{3/2}W_b}\right)\sqrt{\frac{K_BT}{\Delta}}\exp\left(\frac{e\emptyset_m}{K_BT}\right) \times [V_b - (V_b - V_d)\exp\left(-\frac{eV_d}{K_BT}\right)] \tag{14}$$

A. Current density vs. drain voltage

At reasonable values of gate voltages, using Eq. (14), we get

$$J \propto \exp\left(\frac{eV_d}{2K_BT\cosh\,(L_g/2\Lambda)}\right) \times [V_b - (V_b - V_d)\exp\left(-\frac{eV_d}{K_BT}\right) \tag{15}$$

i.e. $J \propto V_d$, if $V_d \leq K_BT/e$ and $J = constant$, if $K_BT/e \ll V_d < V_gW_g/W_b$.

B. Current density vs. gate voltage

At $|V_g| \leq V_bW_g/W_b$,

$$J \propto \exp\,[\frac{V_gW_b}{V_bW_g}] \tag{16}$$

At $|V_g| > V_bW_g/W_b$,

$$J \propto \exp\,[\frac{eV_gW_b}{K_BT(W_b+W_g)}\left(1 - \frac{1}{\cosh\,(L_g/2\Lambda)}\right)] \tag{17}$$

4.0 Results and discussion

The validity of our analytical model is examined by comparing the calculation of I-V characteristics with the corresponding ones of Ref. [18] based on a ‘top of the barrier’ model combined with a tight-binding numerical approach.

4.1 Current in On-Off condition and I_{on}/I_{off}

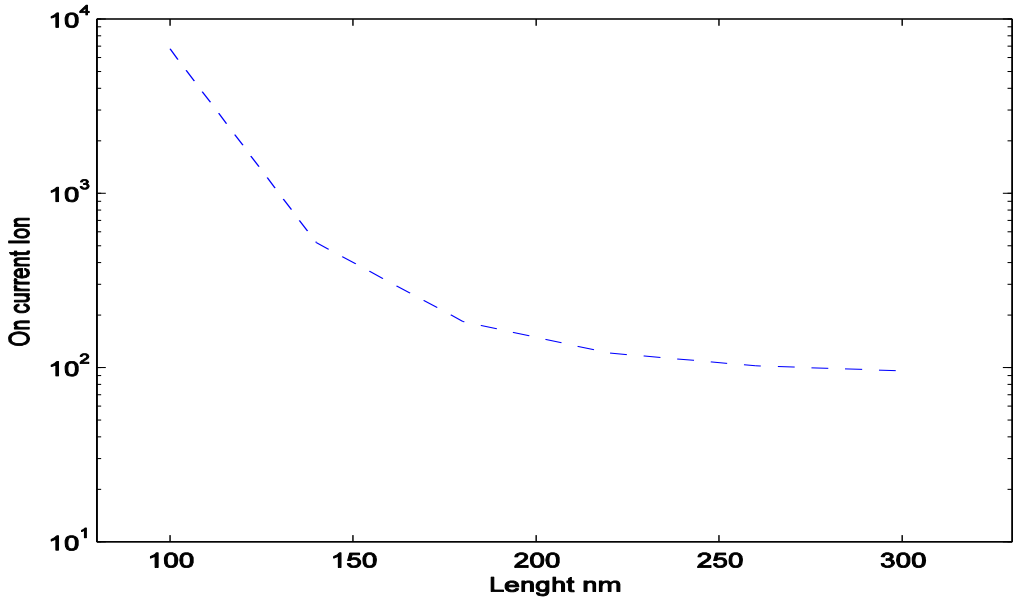

Fig. 4(a). Current in ON condition

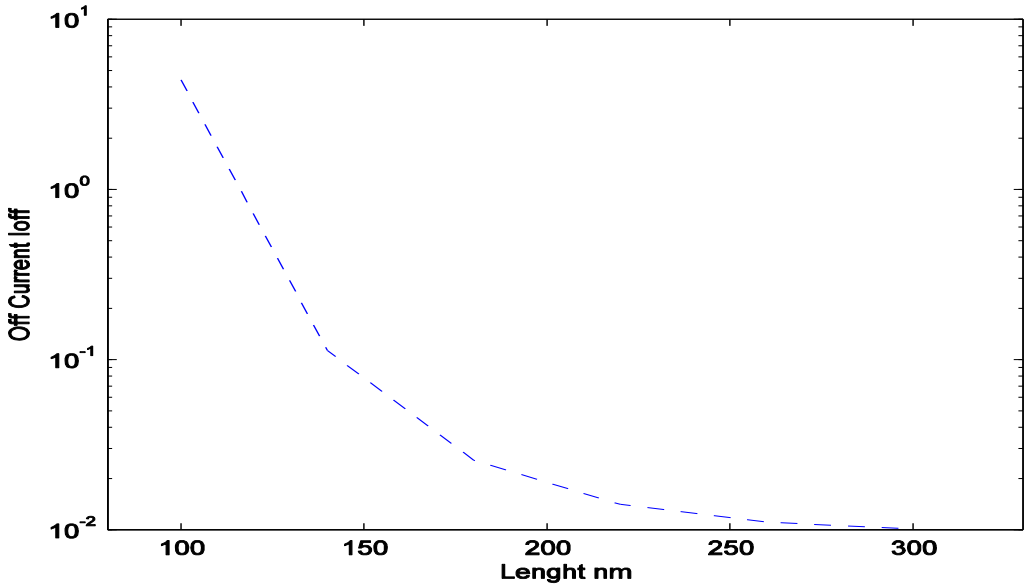

Fig. 4(b). Current in OFF condition

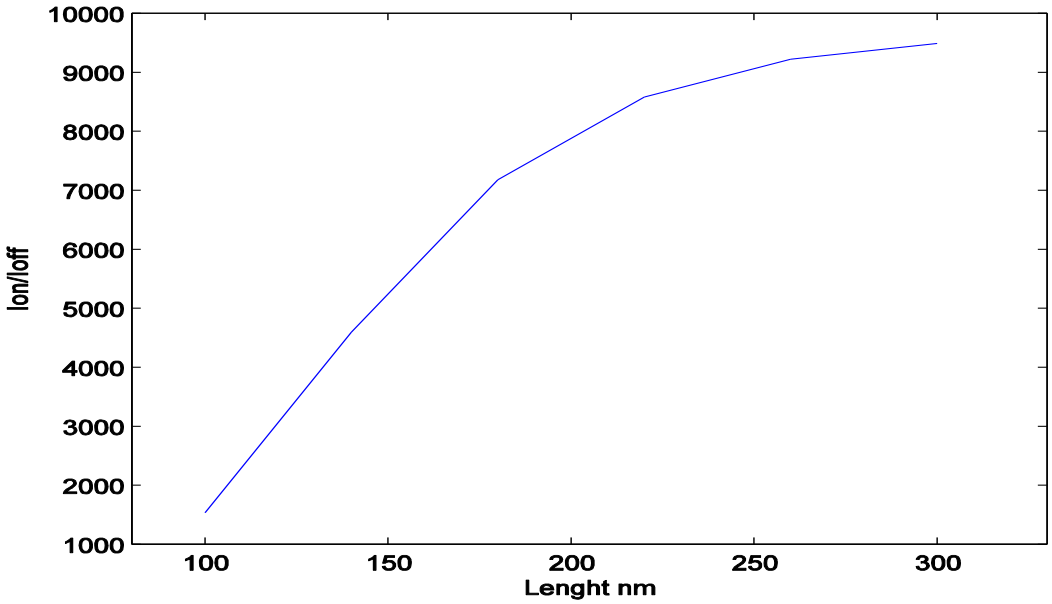

Fig. 4(c). I_{on}/I_{off}

From figure 4(a), 4(b) and 4(c), we observe that I_{off} is steeper than I_{on} and I_{on}/I_{off} is increasing with the increasing of channel length.

4.2 Current density vs. Drain Voltage for different gate voltage

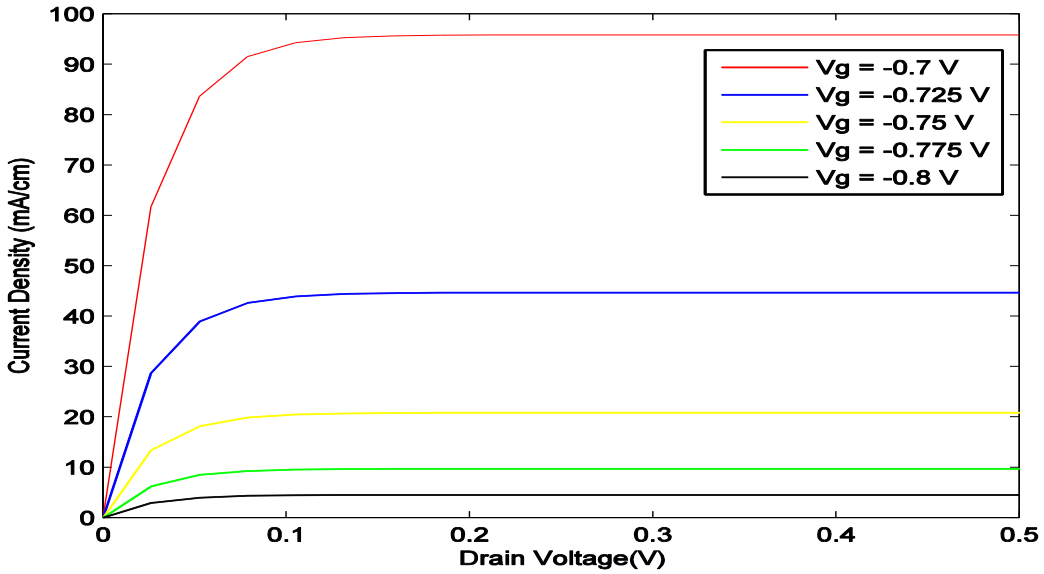

Fig. 5. Current density vs. Drain voltage for different gate voltage, V_g

From figure 5, we can say that current density is increasing with the increase of gate voltage, V_g and drain current is directly proportional to V_g.

4.3 Current density vs. Gate Voltage for different Drain voltage

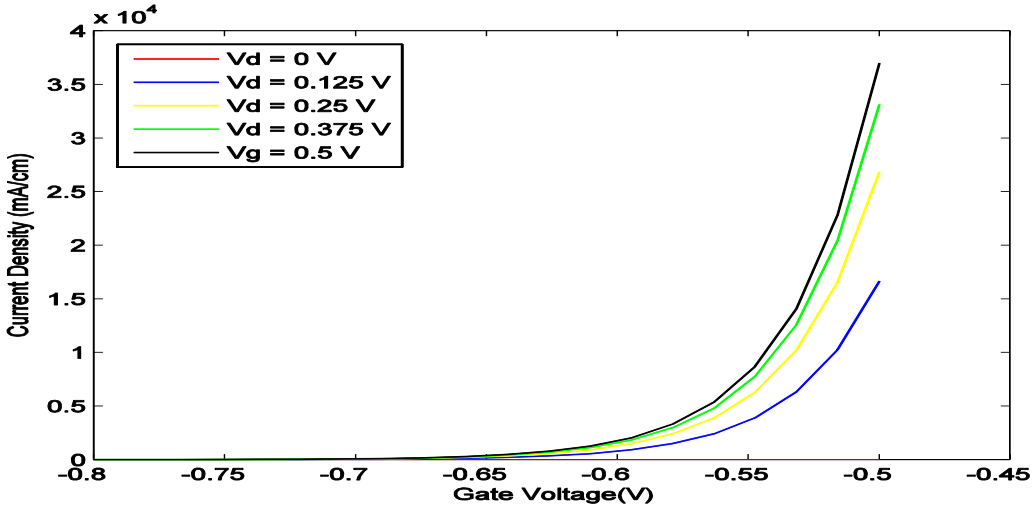

Fig. 6. Current density vs. Gate voltage for different Drain voltage, V_d

From figure 6, we can say that current density is exponentially increasing with the increase of gate voltage, V_g and drain current is directly proportional to drain voltage V_d.

4.4 Current density vs. Drain Voltage for different Energy bandgap

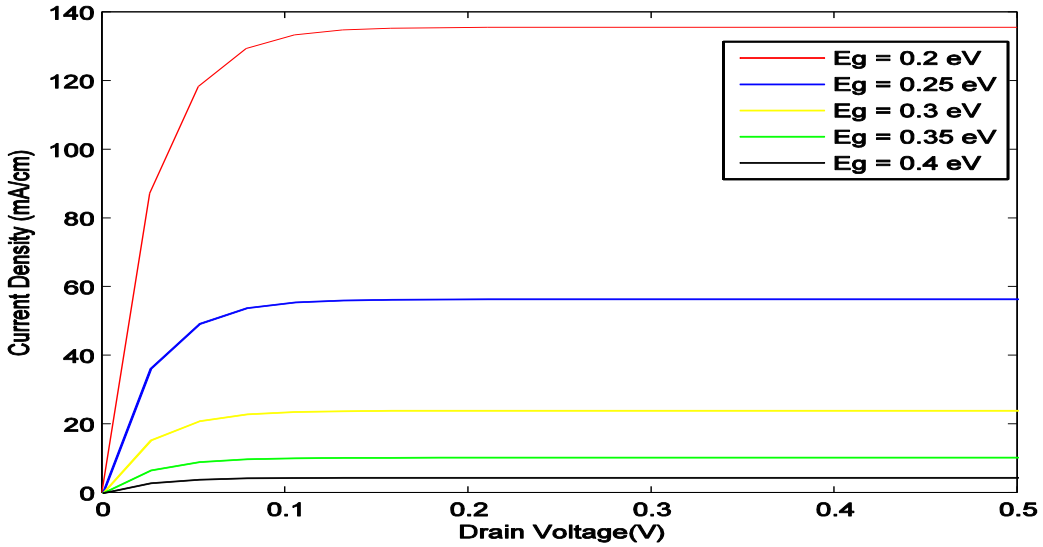

Fig. 7. Current density vs. Drain Voltage for different Energy bandgap

4.5 Current density vs. Gate Voltage for different Energy bandgap

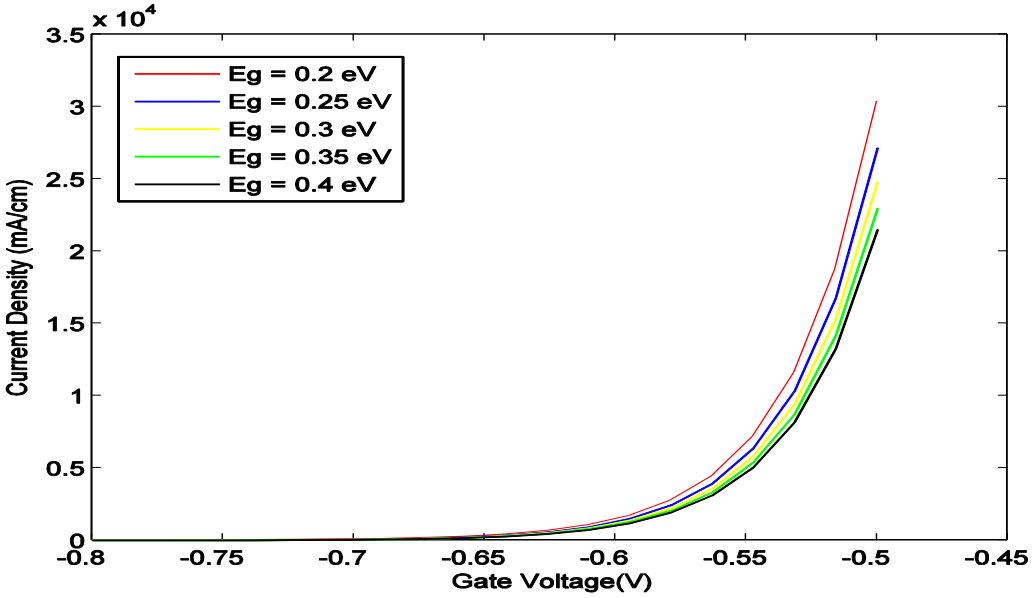

Fig. 8. Current density vs. Gate Voltage for different Energy bandgap

4.6 Current density vs. energy bandgap

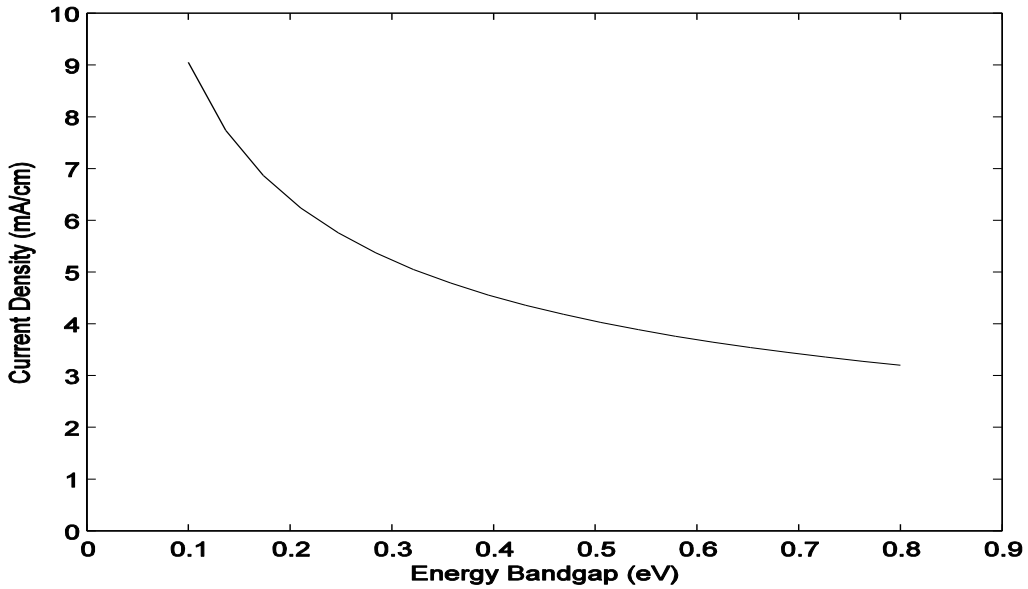

Fig. 9. Current density vs. energy bandgap

From figure 9, we can say that current density is inversely proportional to bandgap.

4.7 Current density vs. Drain Voltage for different channel length

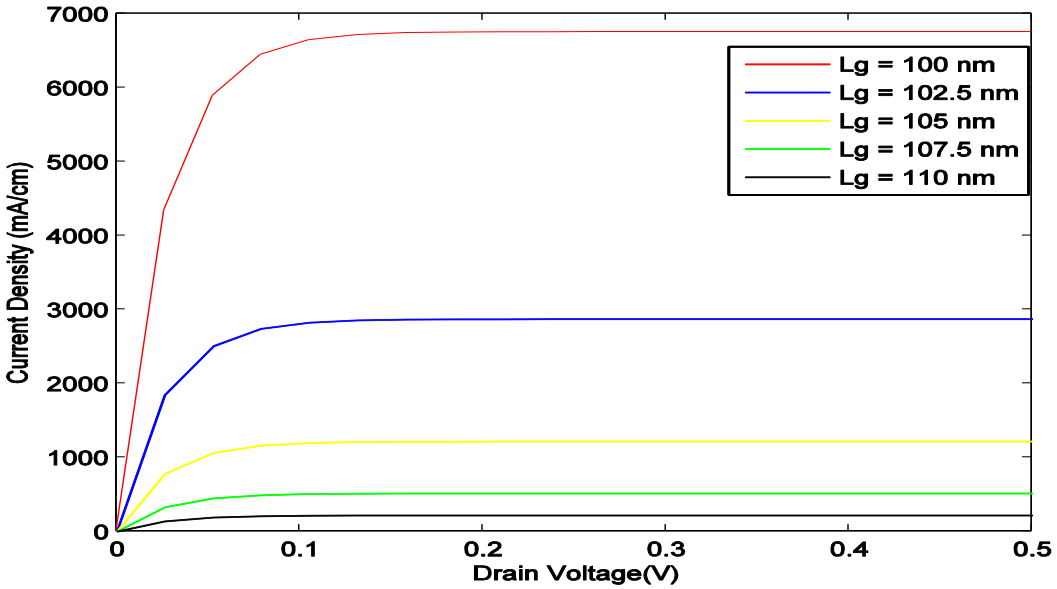

Fig. 10. Current density vs. Drain Voltage for different channel length

4.8 Current density vs. Gate Voltage for different channel length

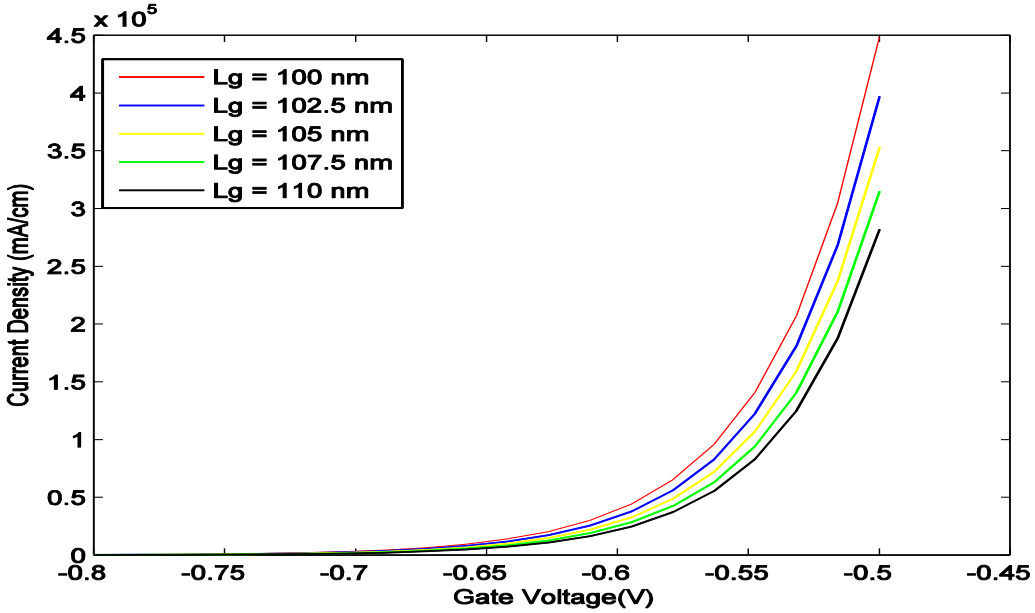

Fig. 11. Current density vs. Gate Voltage for different channel length

4.9 Current density vs. Drain Voltage for different Back gate thickness

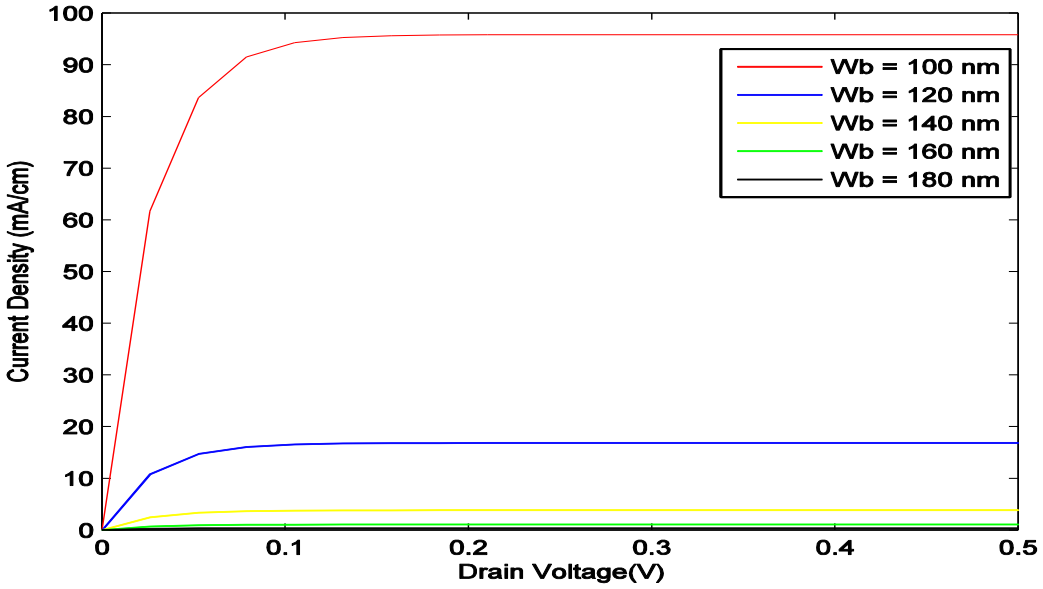

Fig. 12. Current density vs. Drain Voltage for different Back gate thickness

4.10 Current density vs. Gate Voltage for different Back gate thickness

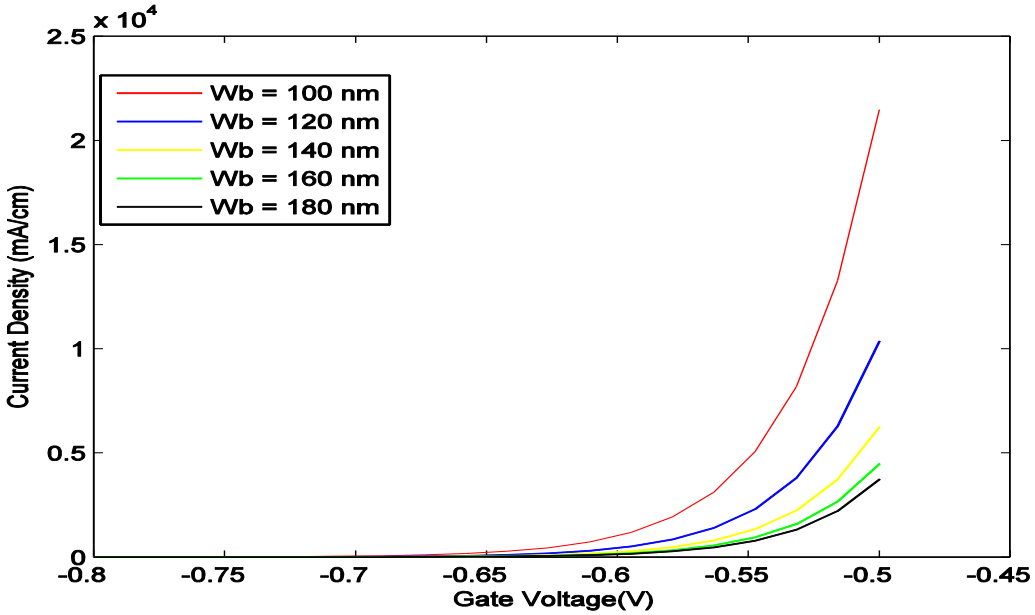

Fig. 13. Current density vs. Gate Voltage for different Back gate thickness

4.11 Current density vs. Drain Voltage for different Top gate thickness

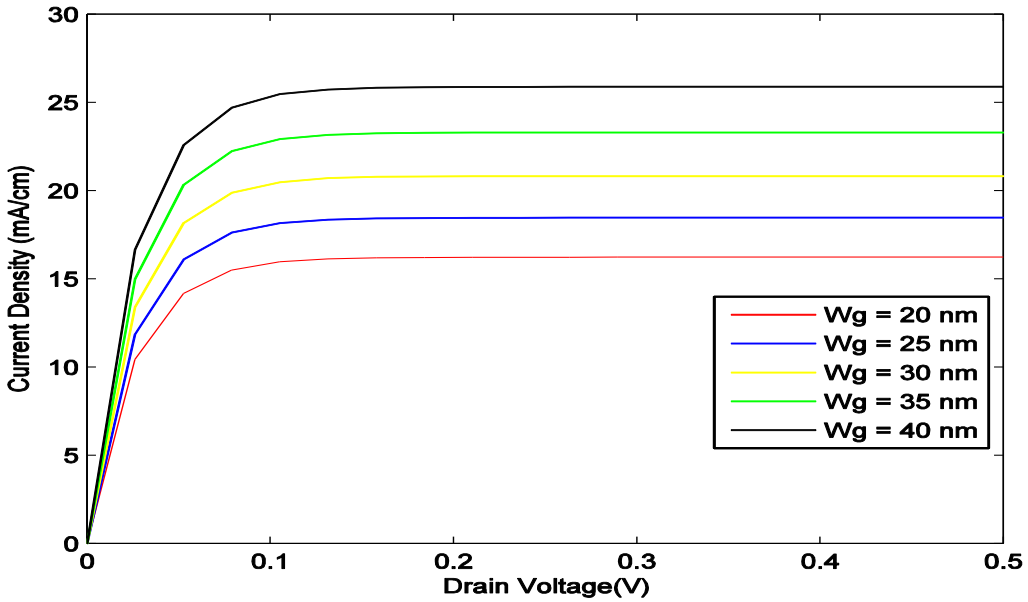

Fig. 14. Current density vs. Drain Voltage for different Top gate thickness

4.12 Current density vs. Gate Voltage for different Top gate thickness

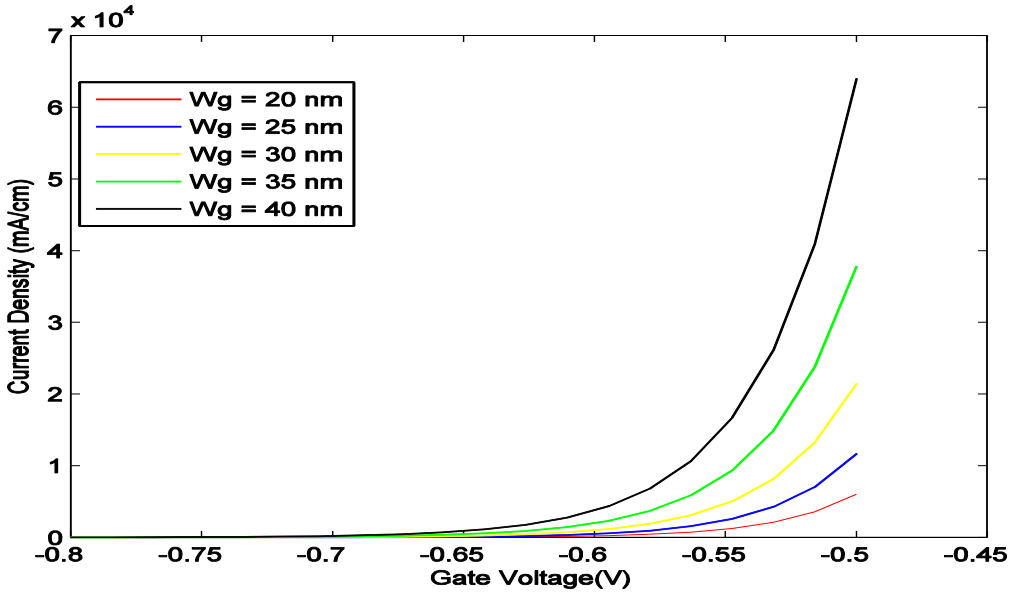

Fig. 15. Current density vs. Gate Voltage for different Top gate thickness

5.0 Conclusion

We have implemented a MATLAB based model for GNRFET. From our observation, we can say that drain current is inversely proportional to bandgap, channel length and back gate thickness, but directly proportional to top gate thickness. In the future, we will work about the applications of GNRFET.

Acknowledgements

The authors acknowledge the contribution of the Department of Electrical and Electronic Engineering, United International University (UIU) and Sonargaon University (SU) for the permission to use computing facilities.

References

[1] Graphene nanoribbons, available online at https://en.wikipedia.org/wiki/Graphene_nanoribbons.
[2] Barone, V., Hod, O., and Scuseria, G. E. (2006), Electronic Structure and Stability of Semiconducting Graphene Nanoribbons, Nano Lett., 6 (12), 2748 - 2754.
[3] Han., M.Y., Özyilmaz, B., Zhang, Y., and Kim, P. (2007), Energy Band-Gap Engineering of Graphene Nanoribbons, Phys. Rev. Lett., 98 (20), 206805-1 – 206805-4.
[4] Tapasztó, L., Dobrik, G., Lambin, P., and Biró, L. P. (2008), Tailoring the atomic structure of graphene nanoribbons by scanning tunnelling microscope lithography, Nat. Nanotech., 3 (7), 397– 401.
[5] Son Y.-W., Cohen M. L., and Louie S. G (2006), Energy Gaps in Graphene Nanoribbons, Phys. Rev. Lett., 97 (21), 216803-1 – 216803-4.
[6] Jung. J., Pereg-Barnea T., and MacDonald A. H. (2009), Theory of Interedge Superexchange in Zigzag Edge Magnetism, Phys. Rev. Lett., 102 (22), 227205-1 – 227205-4.
[7] Huang, L. F., Zhang, G. R., Zheng, X. H., Gong, P. L., Cao, T. F., and Zeng, Z. (2013), Understanding and tuning the quantum-confinement effect and edge magnetism in zigzag graphene nanoribbon, J. Phys., 25 (5), 055304-1 – 055304-8.
[8] Wang, Z. F., Shi, Q. W., Li, Q., Wang, X., Hou, J. G., Zheng, H., Yao, Y., and Chen, J. (2007), Z-shaped graphene nanoribbon quantum dot device, Appl. Phys. Lett., 91 (5), 053109-1 – 053109-3.
[9] Bullis, Kevin (2008), Graphene Transistors, Tech. Review, Cambridge: MIT Technology Review, Inc. Retrieved 2008-02-18.
[10] Bullis, Kevin (2008), TR10: Graphene Transistors, Tech. Review, Cambridge: MIT Technology Review, Inc. Retrieved 2008-02-27.
[11] Wang, X., Ouyang, Y., Li, X., Wang, H., Guo, J., and Dai, H. (2008), Room-Temperature All-Semiconducting Sub-10-nm Graphene Nanoribbon Field-Effect Transistors, Phys. Rev. Lett., 100 (20), 206803-1 – 206803-4.
[12] Ballon, M. S. (2008), Carbon nanoribbons hold out possibility of smaller, speedier computer chips, Stanford Report.
[13] Ismail, R., Ahmadi M. T., and Anwar S., Advanced Nanoelectronics, CRC press, Taylor & Francis Group, London, Chap. 5.
[14] Liang, G., Nikonov, D. E., and Lundstrom, M. S. (2007), Performance projections for ballistic graphene nanoribbon field-effect transistors, IEEE Transactions on Electron Devices, 54(4), 677 – 682.
[15] Zhao, P., Choudhury, M., Mohanram, K., and Guo, J. (2008), Analytical theory of graphene nanoribbon transistors, IEEE International Workshop on Design and Test of Nano Devices, Circuits and Systems, 3 - 6.
[16] Choudhury, M., Yoon, Y., Guo, J., and Mohanram, K. (2008), Technology exploration for graphene nanoribbon FETs, 45th ACM/IEEE Design Automation Conference, 272 - 277.
[17] Yan, Q., Huang, B., Yu, Y., Zheng, F., Zang, J., Wu, J., Gu, B.-L., Liu, F., and Duan, W. (2007), Intrinsic current−voltage characteristics of graphene nanoribbon transistors and effect of edge doping, Nano Lett., 7(6), 1469 – 1473.
[18] Heer, W. A. d., Berger, C., Conrad, E., First, P., Murali, R., and Meindl, J. (2007), Pionics: the emerging science and technology of graphene-based nanoelectronics, IEDM, 199 - 202.